

# Efficient calculations of dispersive properties of photonic crystals using the transmission line matrix method

G. ROMO, T. SMY

Carleton University, Department of Electronics, Ottawa K1S 5B6, ON, Canada;  
e-mail: gluevano@doe.carleton.ca

In this paper, we present an analysis of the accuracy and efficiency of different approaches for the simulation of photonic crystals using the transmission line matrix method. The approaches that we present can be divided into two categories: complex- and real-valued algorithms using a uniform mesh, and complex- and real-valued algorithms using a multigrid mesh. The advantages and disadvantages of each approach are discussed and a brief comparison between these methods is made from the points of view of computational expense and accuracy. It is found that a combination of a real-valued method in a multigrid mesh results in the most efficient algorithm. However, while the complex-valued formulation is valid for the analysis of any photonic crystal, the applicability of the real-valued formulation is limited by structural constraints requiring cell symmetries. It is also found that a multigrid approach can considerably reduce the computational cost required for simulating photonic crystals and our results indicate that a good compromise between accuracy and computational cost can be found. Various photonic crystals are simulated by applying these approaches, and the results are validated using alternative methods.

Keywords: photonic crystals, transmission line matrix (TLM), dispersion relation, multigrid mesh.

## 1. Introduction

The unique property of photonic crystals (PCs) to inhibit the propagation of radiation of certain frequencies, has driven the interest of many researchers worldwide. Thus, a great deal of effort has been set upon the characterization of these structures, as knowledge of the frequencies that will and will not propagate, is indispensable for their practical applications. There exist several methods to obtain this information, and they generally involve the computation of the photonic band structure (or dispersion relation) of the periodic structure.

One of the most widely used methods to compute the photonic band structure of PCs, is the plane wave expansion (PWE) method. This method takes advantage of the fact that both, the solution (electromagnetic fields) and dielectric structure are periodic by expanding them with a Fourier series [1]. This allows Maxwell's equations to be

recast as an eigenvalue problem which is then solved by using standard techniques. Among the advantages of the PWE method are its relative simplicity, accuracy and efficient implementation using fast algorithms [2]. The main disadvantages of this method are that it scales as  $O(N^3)$  where  $N$  is proportional to the size of the problem, and that it cannot deal with lossy dielectric materials.

Another alternative for the computation of the photonic band structure of PCs is to use time domain methods such as finite differences time domain (FDTD) and the transmission line matrix (TLM) method. Unlike the PWE method, time domain methods allow for the straightforward incorporation of material losses into the simulations. In addition, unit cells of arbitrary shapes can be simulated without additional computational effort. In a time domain method, the time required for a calculation scales linearly  $O(N)$  with the number of points used in the discretization [3, 4]. Despite of this, the main drawback of these methods is their long execution time, since very little optimization can be done to reduce the number of operations inherent to the method. Among the time domain methods, the FDTD method is by far the most widely used and has extensively been applied for the analysis and computation of the photonic band structure of PCs [3–9]. The TLM method, on the other hand, has been given very little attention in this respect, despite its increasing popularity for the simulation of general electromagnetic problems [10, 11].

In this paper, we present a number of different approaches for the computation of the photonic band structure of PCs using the TLM method. First, the complex- and real-valued formulations of the TLM method are applied for simulating PCs using a uniform mesh. These formulations are briefly described and their basic advantages and limitations discussed. Next, the complex- and real-valued formulations are revisited using a non-uniform mesh, and the new trade-offs that come into play are also discussed. Thus, the rest of this paper is organized as follows: in Sec. 2, the complex- and real-valued formulations are briefly presented and the limitations of the real-valued formulation are described in detail. In Sec. 3, the procedure for using the non-uniform or multi-grid mesh used in this paper is presented. In Sec. 4, the results of the simulations of various PCs using these different approaches are presented and discussed. Finally, Section 5 presents some conclusions.

## 2. Problem formulation

In this section we describe the basic mathematical concepts governing the simulation of PCs within the formulation of a time method such as TLM. Rather than attempting a rigorous mathematical derivation, the equations are reproduced here only for the sake of completeness. For more details see, for example [12].

From basic solid state physics theory we know that periodic problems have solutions of the form

$$\psi(\mathbf{r}) = u_k \exp(-i \mathbf{k} \cdot \mathbf{r}) \quad (1)$$

where the function  $u_k$  is periodic in space and  $\mathbf{k}$  is a propagation vector. Equation (1) is known as Bloch's theorem, although it is usually referred to as Floquet's theorem in one-dimensional problems. If  $\mathbf{T}$  describes the spatial period of the structure, that is, if it represents a lattice constant vector, then

$$u_k(\mathbf{r} + \mathbf{T}) = u_k(\mathbf{r}). \quad (2)$$

Note that Eqs. (1) and (2) imply that

$$\psi(\mathbf{r} + \mathbf{T}) = \exp(-i\mathbf{k} \cdot \mathbf{T}) \psi(\mathbf{r}), \quad (3)$$

thus, the points  $\mathbf{r}$  and  $\mathbf{r} + \mathbf{T}$  have the same physical properties and the functions differ from each other only by a phase factor. The application of Eq. (3) to the modelling of PCs within the formulation of the TLM method leads to equations of the form [13]

$$V^i(\mathbf{r} + \mathbf{T}) = V^r(\mathbf{r}) \exp(-i\mathbf{k} \cdot \mathbf{T}), \quad (4)$$

$$V^i(\mathbf{r}) = V^r(\mathbf{r} + \mathbf{T}) \exp(i\mathbf{k} \cdot \mathbf{T}),$$

relating the incident and reflected pulses from the boundaries of the simulation domain. In Equation (4)  $V^i$  and  $V^r$  represent the incident and reflected voltage pulses of the nodes on the edge of the simulation domain, respectively. Note that in this equation, the time dependency is not shown, but implicit.

### 2.1. Formulation of a complex-valued TLM algorithm

From Equation (3) we can see that enforcement of the periodicity condition of the fields across the boundaries of the unit cell requires a complex-valued network. In the TLM method, this issue can be dealt with by breaking the periodicity condition into real and imaginary voltage pulses. These voltage pulses are then treated separately throughout the simulation domain and coupled only at the boundaries [14].

When this approach is taken, the periodic boundary conditions in Eq. (4) can be written in terms of the real  $V_{\text{real}}$  and imaginary components  $V_{\text{ima}}$  of the voltage pulses as:

$$\begin{aligned} V_{\text{real}}^i(\mathbf{r} + \mathbf{T}) &= V_{\text{real}}^r(\mathbf{r}) \cos(\mathbf{k} \cdot \mathbf{T}) - V_{\text{ima}}^r(\mathbf{r}) \sin(\mathbf{k} \cdot \mathbf{T}), \\ V_{\text{ima}}^i(\mathbf{r} + \mathbf{T}) &= V_{\text{real}}^r(\mathbf{r}) \sin(\mathbf{k} \cdot \mathbf{T}) + V_{\text{ima}}^r(\mathbf{r}) \cos(\mathbf{k} \cdot \mathbf{T}), \\ V_{\text{real}}^i(\mathbf{r}) &= V_{\text{real}}^r(\mathbf{r} + \mathbf{T}) \cos(\mathbf{k} \cdot \mathbf{T}) + V_{\text{ima}}^r(\mathbf{r} + \mathbf{T}) \sin(\mathbf{k} \cdot \mathbf{T}), \\ V_{\text{ima}}^i(\mathbf{r}) &= -V_{\text{real}}^r(\mathbf{r} + \mathbf{T}) \sin(\mathbf{k} \cdot \mathbf{T}) + V_{\text{ima}}^r(\mathbf{r} + \mathbf{T}) \cos(\mathbf{k} \cdot \mathbf{T}). \end{aligned} \quad (5)$$

In these equations, the superscripts  $i$  and  $r$  stand for incident and reflected voltage pulses of nodes adjacent to the cell boundaries, respectively. Also note that Eqs. (5) are neither subject to approximations nor simplifications, thus its validity holds for unit cells of arbitrary shape and spatial periodicity.

## 2.2. Formulation of a real-valued TLM algorithm

In a real-valued TLM algorithm, the computational effort is reduced by half by restricting the computations to either the real or imaginary part of the complex-valued algorithm. The derivation of a real-valued TLM algorithm was presented in detail in [15] and [16] and, therefore, only the relevant equations will be reproduced here. Within this formulation, the periodicity condition (Eq. (4)) is replaced by:

$$V^i(\mathbf{r}) = \frac{2.0v_1V^r(\mathbf{r} + \mathbf{T}) + V^r(\mathbf{r}) - v_1^2V^r(\mathbf{r})}{v_1^2 + 1.0}, \quad (6)$$

$$V^i(\mathbf{r} + \mathbf{T}) = \frac{v_1^2V^r(\mathbf{r} + \mathbf{T}) - V^r(\mathbf{r} + \mathbf{T}) + 2.0v_1V^r(\mathbf{r})}{v_1^2 + 1.0}. \quad (7)$$

Note that in these equations, the underscripts corresponding to the voltage pulses have been dropped, since all the pulses are known to be real. In addition,  $v_1$  is a phase factor previously introduced in [16].

Although it is not the intention of this paper to compare the performance of the FDTD and TLM methods, it should be noticed at this point that the complex-valued formulation of both methods has a very close resemblance. As a matter of fact, the FDTD counterpart of Eq. (5) can be obtained simply by replacing voltage pulses by electric and magnetic fields in those equations. However, the real-valued TLM algorithm presented in this section proves advantageous, since, to the best of the authors knowledge, it has no straightforward unconditionally stable counterpart in the FDTD method. This is the subject of ongoing research.

In principle, the recursive application of Eqs. (6) and (7) at every time step is sufficient to single out the frequency modes that satisfy the Bloch condition out of a general excitation. However, the use of the real-valued formulation must be done with care due to inherent assumptions.

## 2.3. Limitations of the real-valued algorithm

As it was previously indicated, by using the real-valued TLM algorithm presented in the previous section to calculate the photonic band structure of PCs, the computational effort is reduced by half. However, this advantage is achieved at the expense of introducing some limitations in the definition of the unit cell under simulation.

Consider the one dimensional form of the phase factor presented in [16] such that  $\mathbf{r} = (x_1, y_1, z_1)$  and  $\mathbf{r} + \mathbf{T} = (x_1 + t_x, y_1, z_1)$ . If the spatial period of the structure is

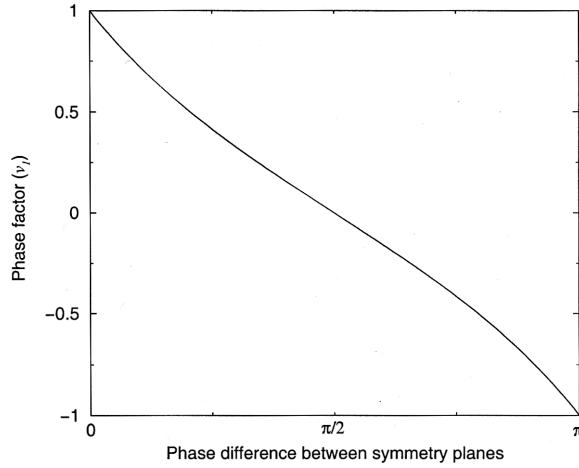


Fig. 1. Phase factor as a function of the normalized propagation vector (phase difference between symmetry planes).

normalized to one ( $t_x = a = 1$ ) and the phase factor  $v_{x,1}$  is graphed as a function of the wave vector value  $k_x$ , the plot shown in Fig. 1 is obtained. Note that the normalization condition of the unit cell implies that the propagation vector numerically equals the phase difference between symmetry planes and can only take values between 0 and  $\pi$ .

Now consider what happens when  $v_1 \equiv v_{x,1}$  is substituted in Eqs. (6) and (7) for three different phase values. For a phase difference of zero, Fig. 1 indicates that  $v_1 = 1$ . Thus Eqs. (6) and (7) reduce to  $V^i(\mathbf{r}) = V^r(\mathbf{r} + \mathbf{T})$  and  $V^i(\mathbf{r} + \mathbf{T}) = V^r(\mathbf{r})$  so that the voltage pulses are just wrapped around the cell without any alterations. Similarly, when the phase difference is equal to  $\pi$ , Fig. 1 indicates that  $v_1 = -1$  and Eqs. (6) and (7) reduce to  $V^i(\mathbf{r}) = -V^r(\mathbf{r} + \mathbf{T})$  and  $V^i(\mathbf{r} + \mathbf{T}) = -V^r(\mathbf{r})$  such that the voltage pulses are now wrapped around but with opposite signs. These results are somewhat intuitive and pose no difficulty to our simulation method. Consider however what happens when the phase difference varies between these two extreme values. Take for example a phase difference of  $\pi/2$ ; for this case,  $v_1 = 0$  and Eqs. (6) and (7) reduce to  $V^i(\mathbf{r}) = V^r(\mathbf{r})$  and  $V^i(\mathbf{r} + \mathbf{T}) = -V^r(\mathbf{r} + \mathbf{T})$ . The fact that the reflected and incident voltage pulses at one end of the simulation domain become equal, implies a *mirror* symmetry plane (or magnetic wall) at that end. Note that this condition holds true regardless of how the unit cell has been defined. In other words, for the results of the simulation to be valid, the unit cell cannot be defined arbitrarily, but it has to be defined such that it is bounded by planes of mirror symmetry. This was made explicitly in [15] where the real-valued formulation was implemented with a magnetic wall on the side of the unit cell.

To illustrate these ideas, consider for example the two-dimensional chessboard PC shown in Fig. 2. Note that for this structure the unit cell can be defined in different, but equivalent ways. For example, the dashed lines in the figure show two possible ways of defining the unit cell.

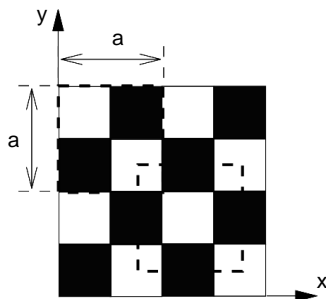


Fig. 2. Simulated two-dimensional chessboard structure. The dashed lines illustrate two possible ways of defining the unit cell.

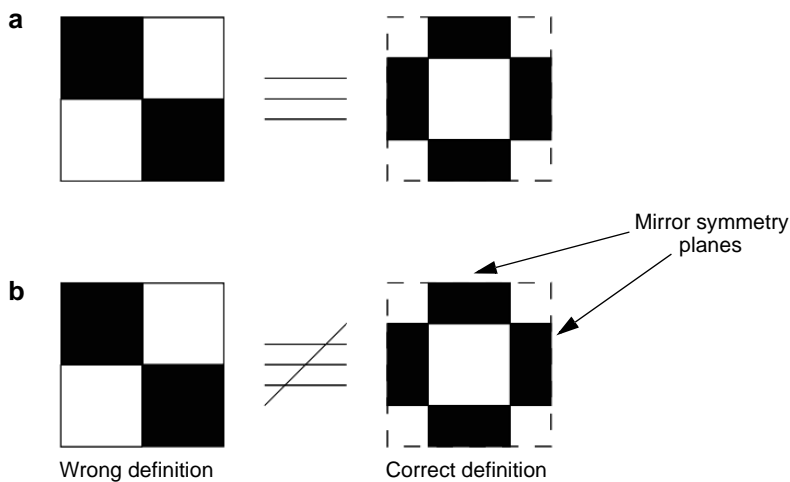


Fig. 3. Unit cell definitions in the complex and real-valued formulations; **a** – alternative definitions are equivalent in a complex-valued formulation; **b** – the definition of the unit cell is restricted to be bounded by mirror symmetry planes in the real-valued formulation.

Based on the previous analysis, the flexibility of defining the unit cell in different ways is only true for the complex-valued formulation. In the real-valued formulation, different unit cell definitions are, in general, not equivalent. This is illustrated in Fig. 3. The fact that the equations imposing the periodicity condition intrinsically contain the assumption that a perfectly symmetric scattering problem (with respect to the edge of the simulation domain) is taking place on “adjacent” cells, is in agreement only with the unit cell definition shown on the right hand side of Fig. 3. Note that this constraint makes the real-valued TLM algorithm not applicable to some PCs because some unit cells do not possess mirror symmetry in all directions (*i.e.*, triangular lattice). However, there is a wide number of PCs and microwave waveguides structures which satisfy the symmetry conditions to be well posed within its formulation.

### 3. Multi-grid approach

In the previous section, the real-valued TLM method was presented as an alternative for reducing the computational effort when computing the photonic band structure of PCs. However, the analysis of the equations enforcing the periodicity condition showed that such an approach can only be applied to unit cells satisfying certain symmetry conditions. Thus, a more general way to proceed toward an efficient computation of the photonic band structure of PCs, is to reduce the number of blocks used for the discretization of the simulation domain. There are two basic ways of accomplishing this: i) to increase the discretization step while maintaining a uniform mesh, and ii) to combine regions with different discretization steps in a multi-grid fashion.

The choice of i) or ii) depends on several factors. While increasing the discretization step results in fewer blocks and therefore faster simulations, it decreases the cut-off frequency of the mesh and increases node dispersion. In addition, the resolution of the mesh is decreased and fine structural details of the cell, cannot be properly represented. In a multigrid mesh, the cut-off frequency is still limited by the biggest block present in the simulation domain, however, it provides the flexibility to properly represent localized structural details where required. This approach is particularly important for the simulation of three-dimensional unit cells of arbitrary shape and large complex structures, where the use of a uniform mesh is computationally prohibited.

The multigrid mesh for the simulation of PCs was implemented using an in-house computer program (Atar). The basic idea behind the model building is to create a complex mesh geometry using rectangular blocks of varying sizes. The model is created such that a block and its neighbors form a relatively simple topology. Each block in the mesh can have either two or four blocks on any side in what is called a quad tree mesh. The mesh is automatically generated based on a set of input parameters such as the minimum and maximum block size, number of levels and location of refinements, *etc.* A constraint that is imposed during the building process for a periodic structure, is that there is a one-to-one correspondence between blocks on opposite sides of the simulation domain. This facilitates the connection of these blocks when enforcing the periodicity condition.

In terms of the TLM method, the small and big internal faces of the blocks are connected using a similar procedure to that described in [17]. The connection procedure is based on ideal matching transformers which preserve the unconditional stability of the TLM method. The basic difference between that formulation and ours, is that in the aforementioned reference, the incident and reflected pulses at the interface are related by circuit-type equations. In our implementation, we relate the pulses by means of a scattering matrix instead. This allows to reduce the number of operations involved in the connection procedure.

## 4. Simulations and evaluation

In this section, we validate the previously described approaches by simulating various PCs. For obtaining the photonic band structures, we used the general procedure described in [16] and more details about the actual implementation can be found in this reference. In all cases, our results were compared with those predicted by the PWE method to verify their validity. Two- and three-dimensional structures were analyzed. For the case of a uniform mesh, the unit cell was discretized into  $32 \times 32 (\times 32)$  uniformly spaced mesh points. In all cases, the lattice constant  $a$  was normalized such that  $a = 1$ . In addition, only TM modes were considered in the two-dimensional structures. That is, the only non-zero field components were the electric field along the infinite dimension and the two magnetic field components transverse to it.

### 4.1. Complex- and real-valued simulations using a uniform mesh

The complex- and real-valued formulations of the TLM method using a uniform mesh were previously presented and validated in [14] and [16], so only the relevant features will be emphasized here.

The first simulated PC was the chessboard structure shown in Fig. 2. This structure has the same symmetry properties as a conventional square lattice. The chessboard structure consisted of an air-dielectric composite and the value of the dielectric material was set to  $\epsilon_r = 11.7$  which corresponds to square pillars of Si connected by the corners and embedded in air. This PC has previously been simulated using the complex-valued TLM method and will be used here, to illustrate the limitations of the real-valued formulation.

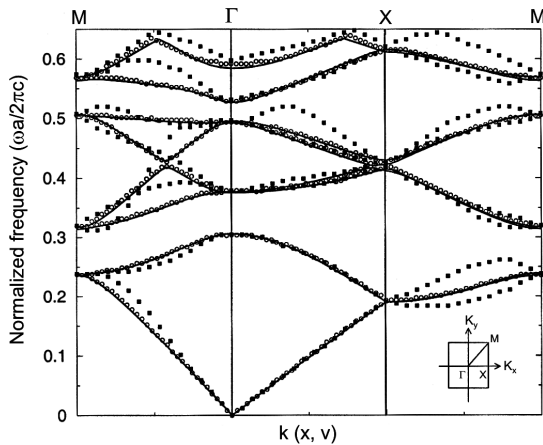


Fig. 4. Dispersion relation of the PC shown in Fig. 3. Circles (filled-squares): simulation results using the real-valued formulation and the unit cell definition shown on the right (left) hand side of Fig. 3. Solid line: PWE method. The inset shows the first Brillouin zone and the symmetry points used for the calculation.

Figure 4 shows a comparison of the dispersion relations of the chessboard structure shown in Fig. 2 obtained by applying the real-valued formulation. The unit cell was defined in two different ways as shown in Fig. 3. The circles correspond to the points predicted by the real-valued formulation using the correct cell definition as shown on the right hand side of Fig. 3, whereas the filled-squares correspond to the points predicted by the same formulation using the incorrect cell definition presented on the left hand side of Fig. 3. In addition, the solid lines show the predictions of the PWE method. As the figure shows, the TLM real-valued formulation and the PWE methods are in good agreement provided that the unit cell is defined such that it is bound by mirror symmetry planes. In the figure, the frequency has been normalized with respect to  $2\pi c/a$  and the inset to it, shows the first Brillouin zone of the chessboard lattice and the symmetry points used for the calculation of the dispersion relation.

It should be emphasized at this point that when the appropriate cell definition is used, the results predicted by the real- and complex-valued formulations are practically indistinguishable from each other. Obviously, this also requires that the two methods be used under the same circumstances (time and discretization steps, number of iterations, TLM-node, *etc.*). Thus, there is a factor of two in the computational effort required by the real and complex-valued formulations when computing the photonic band structure of PCs.

#### 4.2. Complex- and real-valued simulations using a multigrid mesh

In previous sections, it was mentioned that another way to proceed toward a computationally efficient simulation of PCs, is to reduce the number of blocks used for discretizing the simulation domain using a multigrid mesh. In principle, both the complex and real-valued formulations of the TLM method can be applied in a multigrid mesh. However, given that the complex-valued formulation represents the most general scenario, such is the case considered in this section. It should be bear in mind, however, that the results can be extended to the real-valued formulation in the same way as it was done for the case of a uniform mesh.

To illustrate the advantages and disadvantages of a multigrid approach for simulating PCs, we used as a first example, a square lattice of circular rods embedded in air. The dielectric constant of the cylinders was set to  $\epsilon_r = 9.0$  which corresponds to alumina rods embedded in air. The radius of the rods was set to  $0.38a$ , with  $a$  representing the lattice constant. The corresponding unit cell and first Brillouin zone are shown in Fig. 5. In addition, the multi-grid mesh utilized for discretizing the unit cell is shown in Fig. 6. Note that an averaging procedure was applied at the interface between the air and dielectric rods to smooth the transition between the two media. The criterion applied for the discretization of the simulation domain was to limit the refinement to no more than two levels. That is, the multigrid mesh consisted of rectangular blocks formed by the combination of three basic lengths:  $\Delta L$ ,  $2\Delta L$ , and  $4\Delta L$  (where  $\Delta L$  is the step size used for the discretization of the cell using a uniform mesh).

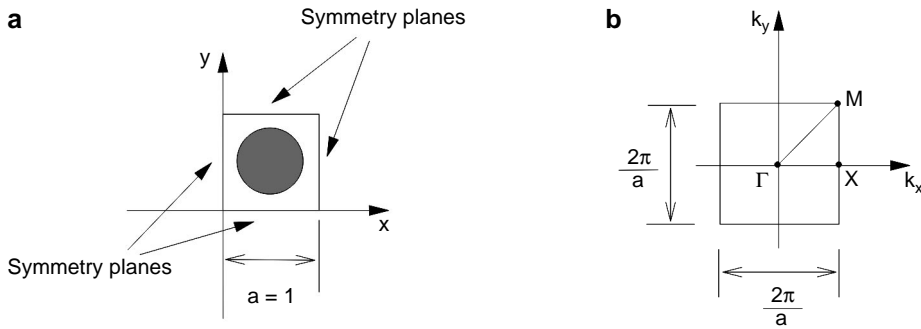


Fig. 5. Unit cell definition (a) and first Brillouin zone (b) of the two-dimensional PC.

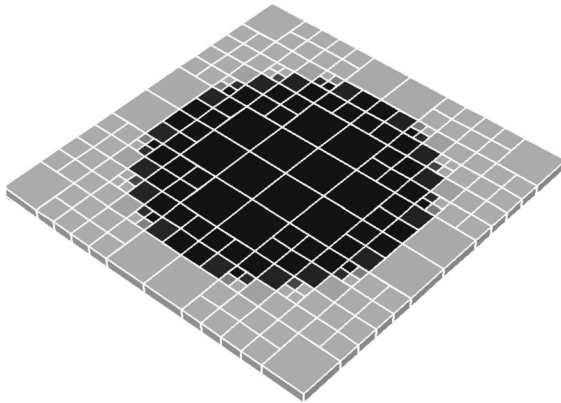


Fig. 6. Multi-grid mesh used for the discretization of the unit cell.

Figure 7 shows a comparison of the dispersion relations of the square lattice of circular pillars obtained by applying three different methods. The dots correspond to the frequency points predicted by the complex-valued formulation using a uniform mesh. In addition, the filled-squares represent the frequency points predicted by the complex-valued formulation using the multigrid mesh of Fig. 6. In the figure, the frequency has been normalized as before. As a way of comparison, the solid lines show the results predicted by the PWE.

As Fig. 7 shows, the overall agreement between the three different approaches is fairly good. However, the introduction of a coarser mesh has slightly degraded the accuracy of the TLM method as expected. The accuracy of the results were mainly affected by two sources of error: node dispersion and meshing error. Node dispersion relates to the fact that short wavelengths (compared with the block size) are not properly represented by the mesh. As a result, the wave velocity becomes dispersive and dependent on the direction of the propagation vector. Meshing error refers to the degree of accuracy with which structural details of the unit cell and dense fields are represented in the mesh. Naturally, the multigrid mesh can be devised so that the

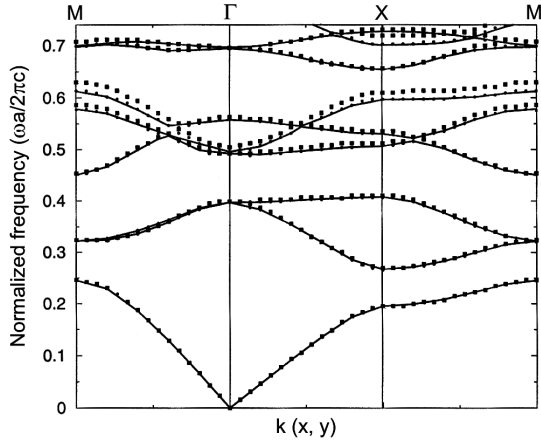


Fig. 7. Dispersion relation of the PC shown in Fig. 3. Dots: simulation results using the  $R$ - $V$  formulation in a uniform mesh. Filled-squares: simulation results using a  $C$ - $V$  formulation in a multi-grid mesh. Solid line: PWE method.

structural details of the cell are properly represented in the mesh. However, there is no guarantee that the resulting mesh will properly represent the field modes in all regions. As a consequence, field meshing error is still present in the multigrid mesh.

Note that, while it is generally true that in a multigrid mesh the maximum error occurs at higher frequencies, our present example shows that this is not necessarily the case. For the present photonic band structure, the worst discrepancy between frequency modes predicted by the uniform and multigrid meshes occurred near the ends of the sixth band, with an error of approximately 2.7%. Also note that the predictions of the multigrid mesh are in good agreement for frequencies well above the theoretical cut-off frequency of the mesh ( $\sim 0.26$  units of normalized frequency). For this example, the discretized structure consisted of  $220$  blocks. Thus, when compared with a  $32 \times 32$  uniform mesh, the computational efficiency is increased by a factor of 4.65.

The efficiency of time-domain methods is directly related to the number of blocks used to build the model. Thus, a multigrid mesh is a natural approach to reduce the number of blocks and hence the computational effort. However, there is a large number of ways in which a multigrid mesh can be defined to discretize a given PC. Thus, while it is not possible to characterize all the different multigrid meshes individually, they can be characterized collectively by the minimum and maximum block size present in the mesh. The minimum block size determines the spatial resolution and the maximum block size, the cut-off frequency of the mesh.

The real advantage of a multigrid mesh is better appreciated in larger problems. To illustrate this point, the next simulated example is a three-dimensional one. For this case, we chose a structure consisting of dielectric spheres embedded in air. The dielectric constant of the spheres was set to 12.0 and their radius to  $0.3125a$ . To also illustrate the trade-offs that come into play when multi-gridding is used, two different

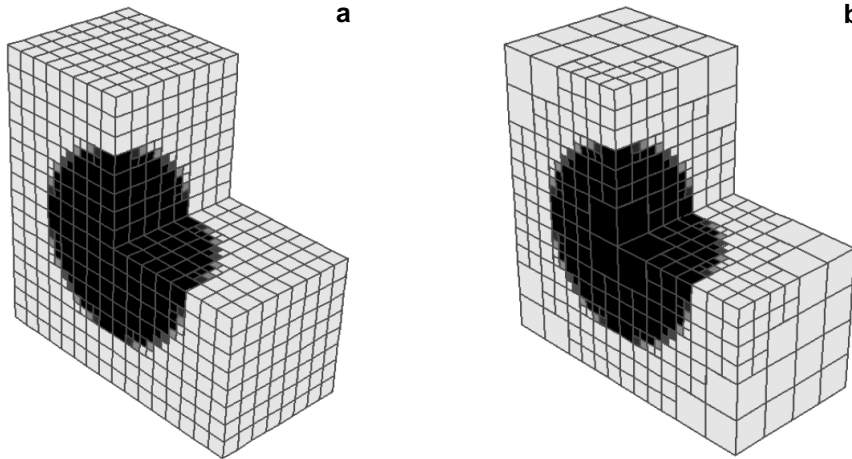


Fig. 8. Multigrid meshes used for the discretization of the unit cell. The maximum block has been limited to: **a** –  $1/16$  and **b** –  $1/8$ .

meshes are looked at. Figure 8 shows the multigrid meshes that were used for the discretization of the unit cell. In Figs. 8a and 8b, one and two levels of refinement were allowed respectively during the generation of the mesh. Thus, while the spatial resolution is the same for both meshes (equal to  $1/32$ ), the cut-off frequency of the mesh in Fig. 8b is half that of the mesh in Fig. 8a. In what follows, we will denote these meshes as Multigrid-( $1/16$ ) and Multigrid-( $1/8$ ), respectively, where the number in parentheses denotes the maximum block size (remember that the lattice constant has been normalized to  $a = 1$ ). Similarly to the previous example, an averaging procedure was applied to smooth the transition between the dielectric spheres and the air. In addition, Figs. 8a and b show that three-dimensional structures favor the formation of cubic, rather than rectangular blocks during the building process.

Figure 9a shows the photonic band structure of the cubic lattice of dielectric spheres. The corresponding first Brillouin zone and symmetry points used as a reference for the computation of the band structure are shown in Fig. 9b. The solid lines were obtained by using a computer program based on the PWE method in a uniform mesh [2]. The open circles represent the frequency points predicted by the complex-valued TLM formulation using the Multigrid-( $1/16$ ) for discretizing the unit cell. Similarly, the filled-squares represent the frequency points predicted by the complex-valued TLM formulation when the Multigrid-( $1/8$ ) is used. For the Multigrid-( $1/16$ ), the simulation domain consisted of 5776 blocks. This indicates that the computational efficiency is increased by a factor of 5.7 when compared with a  $32 \times 32 \times 32$  uniform mesh.

In terms of accuracy, Fig. 9a shows that the agreement between the uniform and multigrid meshes is fairly good up to the frequency shown in the figure. This is true despite the fact that, strictly speaking, the cut-off frequency of the Multigrid-( $1/16$ ) is only  $\sim 0.46$  units of normalized frequency. In calculating this frequency, a minimum of ten nodes per wavelength has been used as a reference. In addition, it has been

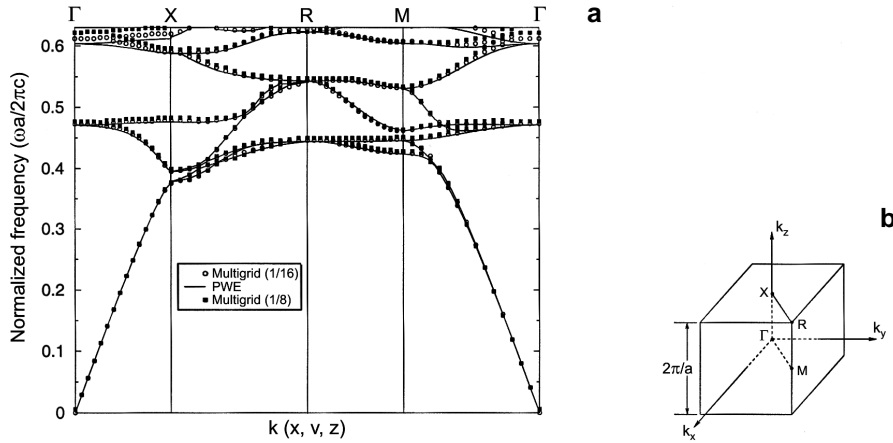


Fig. 9. Dispersion relation of the simple cubic lattice; filled-squares: Multigrid-(1/16) mesh; open circles: Multigrid-(1/8); solid lines: PWE method using a uniform mesh (a) and first Brillouin zone of the simple cubic lattice (b).

calculated with respect to the dielectric sphere, where the shorter wavelengths (for a fixed frequency) are expected.

When the Multigrid-(1/8) was used to discretize the unit cell, the resulting structure consisted of 3928 blocks. In this case, the computational efficiency is increased by a factor of 8.3 when compared with a  $32 \times 32 \times 32$  uniform mesh. As expected, the addition of bigger blocks in the simulation domain has further degraded the accuracy of the results. However, we can see from Fig. 9a that although the cut-off frequency of this mesh is only  $\sim 0.23$  units of normalized frequency, the results are in good agreement up to at least two times this value. We can also see that the worst discrepancy between the uniform and multigrid methods occurred near the ends of the upper most bands. That is, when one (or more) of the components of the propagation vector is equal to zero. This is again, an expected result, since it is known that block dispersion is worst under this scenario [18]. It should be pointed out that these results were obtained by using a stub-loaded node and are expected to improve, due to superior node dispersion properties, by using hybrid or super condense nodes [19].

Figure 10 shows the computational time associated with the various methods presented in this paper as a function of the spatial resolution of the mesh (minimum block size). In the figure, the computational time has been normalized with respect to the complex-valued TLM method applied in a uniform mesh, which is the slowest, but most accurate scenario. This method is indicated by the dashed line in the figure. Similarly, the dot-dashed line represents the computational time of the real-valued TLM method also applied in a uniform mesh. As it was explained before, this method reduces the computational effort by half as compared with the complex-valued formulation while retaining the same accuracy. The two remaining lines in the figure show the results of the multigrid approach. As the figure indicates, two cases were considered. The solid and dotted lines correspond to multigrid meshes where the

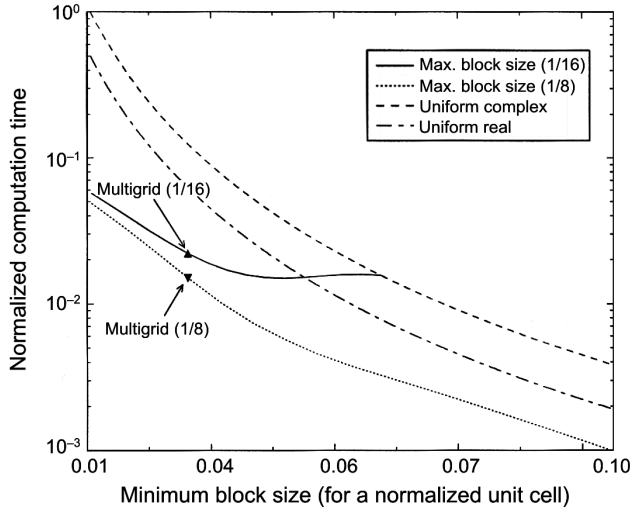


Fig. 10. Computational time as a function of minimum block size for the various methods. Dashed (dot-dashed) line: complex (real)-valued formulation in a uniform mesh; solid and dashed lines: complex-valued formulation in a multigrid mesh, the maximum block size is limited to 1/16 and 1/8, respectively.

resolution is varied while the maximum block size is limited to 1/16 and 1/8, respectively. In the figure, the corresponding locations of the multigrid meshes shown in Fig. 8 are also indicated.

Figure 10 shows that the computational efficiency of a multigrid approach is enhanced toward higher resolutions (smaller block size). This is particularly important for the simulation of PCs because it is in this region where the cut-off frequency of a uniform mesh is unnecessarily high ( $>1$  unit of normalized frequency). This translates into the possibility of finding a good compromise between computational time and accuracy. It should be noted that the computational time associated with the multigrid method could further be reduced by half, if the geometry of the unit cell allowed for the real-valued formulation to be used.

The results presented in this section indicate that a multigrid approach can considerably reduce the simulation time that is required for computing the photonic band structure of PCs while maintaining a good accuracy.

## 5. Conclusions

In this paper, different approaches for the simulation of PCs using the TLM method were presented. These approaches were divided into complex- and real-valued algorithms using a uniform mesh, and complex- and real-valued algorithms using a multigrid mesh. The advantages and disadvantages of each approach were discussed and a comparison between these methods was made from the points of view of computational expense and accuracy.

It was found that a combination of a real-valued method in a multigrid mesh results in the most efficient algorithm. However, unlike the complex-valued formulation, its applicability is limited to unit cells satisfying certain geometrical details. It was also found that while a multigrid approach can considerably reduce the computational effort required for simulating PCs, it also reduces the accuracy of the results. In this respect, our results indicate that a good compromise between execution time and accuracy can be found when using the multigrid approach. In addition, it was observed that the multigrid meshes presented in this paper had a good performance, well above the typical theoretical cut-off frequency of the mesh.

*Acknowledgements* – This work was supported by the Natural Sciences and Engineering Research Council of Canada (NSERC), the Microelectronics Network within the Canadian Federal Networks of Centers of Excellence Program (MICRONET), The Canadian Institute for Photonic Innovations (CIPI) and EMPWR.

## References

- [1] SAKODA K., *Optical Properties of Photonic Crystals*, Springer, Germany 2001.
- [2] JOHNSON S.G., JOANNOULUS J.D., *Block-iterative frequency-domain methods for Maxwell's equations in a planewave basis*, Optics Express **8**(3), 2001, pp. 173–190.
- [3] CHAN C.T., YU Q.L., HO K.M., *Order-N spectral method for electromagnetic waves*, Physical Review B: Condensed Matter **51**(23), 1995, pp. 16635–42.
- [4] WARD A.J., PENDRY J.B., *A program for calculating photonic band structures, Green's functions and transmission/reflection coefficients using a non-orthogonal FDTD method*, Computer Physics Communications **128**(3), 2000, pp. 590–621.
- [5] YAMADA S., WATANABE Y., KATAYAMA Y., COLE J.B., *Simulation of optical pulse propagation in a two-dimensional photonic crystal waveguide using a high accuracy finite-difference time-domain algorithm*, Journal of Applied Physics **93**(4), 2003, pp. 1859–64.
- [6] THÉVENOT M., REINEIX A., JECKO B., *FDTD approach for modelling PBG structures*, Journal of Optics A: Pure and Applied Optics **1**(4), 1999, pp. 495–500.
- [7] MEKIS A., FAN S., JOANNOPOULOS J.D., *Absorbing Boundary Conditions for FDTD Simulations of Photonic Crystal Waveguides*, IEEE Microwave and Guided Wave Letters **9**(12), 1999, pp. 502–4.
- [8] CHUTINAN A., NODA S., *Waveguides and waveguide bends in two-dimensional photonic crystal slabs*, Physical Review B: Condensed Matter **62**(7), 2000, pp. 4488–92.
- [9] QIU M., AZIZ K., KARLSSON A., SWILLO M., JASKORZYNSKA B., *Numerical studies of mode gaps and coupling efficiency for line-defect waveguides in two-dimensional photonic crystals*, Physical Review B: Condensed Matter and Materials Physics **64**(15), 2001, pp. 155113/1–5.
- [10] ABU EL-HAJJA A.J., *Analysis of the optical properties of thin films using the transmission line method*, Optica Applicata **27**(2), 1997, pp. 121–41.
- [11] JACQUIN O., HDAGUJIMANA F., CACHARD A., BENECH P., *Application of the TLM technique to integrated optic component modelling*, International Journal of Numerical Modelling: Electronic Networks, Devices and Fields **14**(2), 2001, pp. 95–105.
- [12] COLLIN R.E., *Field Theory of Guided Waves*, 2nd Ed., NJ: IEEE Press, Piscataway 1991.
- [13] CELUCH-MARCYSIAK M., GWAREK W.K., *Spatially looped algorithms for time-domain analysis of periodic structures*, IEEE Transactions on Microwave Theory and Techniques **43**(4), 1995, pp. 860–5.
- [14] ROMO G., SMY T., *Dispersion relation calculation of photonic crystals using the transmission line matrix method*, International Journal of Numerical Modelling: Electronic Networks, Devices and Fields **17**(5), 2004, pp. 451–9.

- [15] WALTER M., PERTZ O., BEYER A., *A contribution to the modeling of longitudinally periodic waveguides by the help of the TLM method*, IEEE Transactions on Microwave Theory and Techniques **48**(9), 2000, pp. 1574–6.
- [16] ROMO G., SMY T., *Modeling of photonic crystals using a real-valued transmission line matrix method*, Journal of Applied Physics **94**(4), 2003, pp. 2177–82.
- [17] WŁODARCZYK J., *New multigrid interface for the TLM method*, Electronics Letters **32**(12), 1996, pp. 1111–12.
- [18] CHRISTOPOULOS C., *The Transmission-Line Modeling Method TLM*, NJ: IEEE Press, Piscataway 1995.
- [19] TRENTIK V., CHRISTOPOULOS C., BENSON T.M., *Development of a general symmetrical condensed node for the TLM method*, IEEE Transactions on Microwave Theory and Techniques **44**(12), 1996, pp. 2129–35.

*Received November 4, 2004*